Applied Energy 87 (2010) 2304–2312

Contents lists available at ScienceDirect

Applied Energy

journal homepage: www.elsevier.com/locate/apenergy

Maximum-power-point tracking with reduced mechanical stress applied to wind-energy-conversion-systems

L.G. González [a,*], E. Figueres [b], G. Garcerá [b], O. Carranza [c]

[a] Departamento de Electrónica y Comunicaciones, Universidad de los Andes, núcleo la Hechicera, 5101 Mérida, Bolivarian Republic of Venezuela
[b] Grupo de Sistemas Electrónicos Industriales, Universidad Politécnica de Valencia, Camino de vera s/n, 46022 Valencia, Spain
[c] Escuela Superior de Computo, Instituto Politécnico Nacional, Av. Juan de Dios Bátiz s/n, 07738 DF, Mexico

ARTICLE INFO

Article history:
Received 1 September 2009
Received in revised form 11 November 2009
Accepted 23 November 2009
Available online 6 January 2010

Keywords:
Wind-energy-conversion-systems
Maximum-power-point tracking
Perturbation-observation-method
Mechanical stress

ABSTRACT

This paper presents an improved maximum-power-point tracking algorithm for wind-energy-conversion-systems. The proposed method significantly reduces the turbine mechanical stress with regard to conventional techniques, so that both the maintenance needs and the medium time between failures are expected to be improved. To achieve these objectives, a sensorless speed control loop receives its reference signal from a modified Perturb&Observe algorithm, in which the typical steps on the reference speed have been substituted by a fixed and well-defined slope ramp signal. As a result, it is achieved a soft dynamic response of both the torque and the speed of the wind turbine, so that the whole system suffers from a lower mechanical stress than with conventional P&O techniques. The proposed method has been applied to a wind turbine based on a permanent magnet synchronous generator operating at variable speed, which is connected to the distribution grid by means of a back to back converter.

1. Introduction

The use of renewable energy has been increased in the last decade due to the high cost of fossil fuels and the different agreements among the industrialized countries with the aim of reducing CO_2 emissions. Particularly, wind-energy-conversion-systems (WECS) are considered as the most cost effective of all the currently exploited renewable sources [1]. In fact, some countries like Germany, USA and Spain get a considerable amount of generated power from WECS, which is getting comparable to conventional generation sources.

In the design of WECS, two major issues may be pointed out. The first one is the variable and unpredictable availability of the wind. The second one is the strong dependence that it exists between the turbine aerodynamics, the generator speed and the amounts of power that may be extracted from the wind. Therefore, the use of a maximum-power-point tracking (MPPT) algorithm [2–4] is mandatory to extract as much power as possible from the wind when it becomes available. MPPT algorithms may work at an almost constant generator speed by actuating on the turbine aerodynamics, but the use of variable speed systems increases the global conversion efficiency [5]. Additionally, the costs of the WECS can be reduced if a fixed pitch angle is chosen.

A large number of MPPT techniques has been proposed for both photovoltaic [6,7] and wind generators [4,8,9]. Some of them need an accurate knowledge of the turbine parameters and the measurement of the wind speed to calculate the value of the speed generator that allows operating close to the maximum power point (MPP) [8]. Therefore, they are sensitive to modeling uncertainties and may become ineffective in some cases. An interesting method to achieve MPPT in wind turbines is the so called Perturb&Observe algorithm (P&O) [10]. This technique has been extensively used in power processing of photovoltaic panels. In the context of variable speed WECS, P&O continuously modifies the turbine operation point, by increasing or decreasing the generator speed following the sign of the measured power variations. As a result, MPPT can be achieved without the need of either an accurate knowledge of the turbine parameters or the actual wind speed. However, because of the wind turbine characteristics, small changes in the generator speed may result in large variations of the torque that is applied to the mechanical transmission among the wind turbine and the electrical generator [2,3]. This fact could increase the maintenance needs and reduce the medium time between failures (MTBF) of the WECS, so that the exploitation benefits may be compromised. To solve this problem, an adaptive P&O was proposed in [3] to reduce the size of the speed steps when the WECS is close to an MPP. Unfortunately, with strongly varying wind conditions the maximum power operation point can change quickly, so that the mechanical stress may be not significantly reduced. Another approach was proposed in [11], where low-pass filters were added

* Corresponding author.
E-mail address: lgerardo@ula.ve (L.G. González).

0306-2619/$ - see front matter © 2009 Elsevier Ltd. All rights reserved.
doi:10.1016/j.apenergy.2009.11.030

to the speed controller to achieve a soft dynamic response of the WECS.

It is worth to point out that the energy available at high wind speeds may exceed the maximum power that it can be processed by the WECS. When this situation appears, the MPPT operation mode must be stopped and the extracted power must be limited to the nominal one of the WECS. This mode of operation is called constant power region (CPR).

This work presents a modification of the conventional P&O algorithm applied to WECS, in which the typical steps on the reference speed have been substituted by a fixed and well-defined slope ramp signal. The goal of this modification is to achieve a soft transition between two algorithm iterations, so that the generator torque response is less aggressive and therefore, the mechanical transmission stress among the wind turbine and the electrical generator is significantly reduced. From an applied point of view, the consequence of the proposed method is that both the maintenance needs and the MTBF of the WECS are expected to be improved, so that the exploitation benefits can be increased. Moreover, to avoid the additional costs associated to the use of speed sensors, a sensorless technique based on a simplified Kalman filter [12] has been chosen to close the turbine speed control loop. Besides, a variable control structure that was proposed in [13] has been used to eliminate the P&O steps when the turbine works into CPR. Conventionally, in this operation mode the P&O algorithm is modified to limit the extracted power below the nominal one of the system. As a result, the steps on the speed reference do not drive the turbine to the maximum point of the power vs. speed characteristic, but to a point that is limited by the nominal power of the WECS. With the proposed approach, a linear power control loop is used to maintain the extracted power close to the nominal one, so that the reference for the speed control loop follows the output of a relatively slow power controller instead the steps calculated by the P&O algorithm. It is worth pointing out that the mechanical stress in the CPR operation mode is also reduced by applying the proposed variable control structure. A detailed description of the design of the linear power control loop may be found in [13].

The proposed techniques have been applied to a WECS based on a PMSG operating at variable speed, which is connected to the distribution grid by means of a back to back converter (see Fig. 1). In variable speed wind generation systems it is usual to choose a permanent magnet synchronous generator (PMSG) because, among other advantages, the use of a gearbox can be avoided. The control of the grid side inverter is out of the scope of this paper, but a detailed description may be found in [14].

The paper is organized as follows. Section 2 presents a small-signal model of both the PMSG and the aerodynamic characteristics of the wind turbine. Section 3 shows the analysis and design of the speed control loop. The dynamic response of the turbine power to changes in the reference speed is also analyzed in Section 3. Section 4 describes both the conventional and the proposed P&O algorithms. In Section 5 some simulations results are presented, showing the response of the proposed control scheme to wind speed variations. Finally, in Section 6 some conclusions are outlined about the performance achieved by the proposed P&O algorithm with regard to the conventional one.

2. Small-signal modeling of permanent magnet synchronous generators and wind turbines

2.1. Permanent magnet synchronous generators model

Fig. 2a and Eq. (1) show a model of PMSG with a sinusoidal flux distribution, represented in a stationary three-phase frame [15]. R_s and L are the stator resistance and inductance, respectively. u_a is the phase to neutral terminal voltage and e_a is the phase to neutral electromotive force (EMF) driven by the permanent magnets. After applying Park's transform, Eqs. (2) and (3) result, which represent a model of the PSMG in a synchronous reference frame, also called the d–q frame. Fig. 2b shows the corresponding equivalent circuit. Note that, because of the large value of the PMSG inductances, the output voltage of the generator can be directly connected to the rectifier, avoiding the use of additional filter inductors.

$$\frac{d}{dt}\begin{bmatrix} i_a \\ i_b \\ i_c \end{bmatrix} = -\frac{R_s}{L}\begin{bmatrix} i_a \\ i_b \\ i_c \end{bmatrix} + \frac{1}{L}\begin{bmatrix} e_a \\ e_b \\ e_c \end{bmatrix} - \frac{1}{L}\begin{bmatrix} u_{sa} \\ u_{sb} \\ u_{sc} \end{bmatrix} + \frac{V_n}{L} \tag{1}$$

$$u_{sd} = -R_s i_{sd} + \omega_e \psi_{sq} - \dot{\psi}_{sd} \tag{2}$$

$$u_{sq} = -R_s i_{sq} + \omega_e \psi_{sd} - \dot{\psi}_{sq} \tag{3}$$

Both d and q components of the stator induced flux are described by Eqs. (4) and (5). u_{sd} and u_{sq} are the stator terminal voltages, I_{sd} and I_{sq} are the stator currents, Ψ_{PM} is the magnetic flux produced by the permanents magnets, and L_d and L_q are the equivalent stator inductances in the dq synchronous reference system.

$$\psi_{sd} = L_d i_{sd} - \Psi_{PM} \tag{4}$$

$$\psi_{sq} = L_q i_{sq} \tag{5}$$

The electrical torque applied to the PMSG rotor is represented by (6), where P is the number of the machine poles. By considering a PMSG without rotor saliency (where $L_d = L_q$), and applying the so called $I_{sd} = 0$ technique [16], the expression of the generator torque can be simplified as expressed by Eq. (7). As a consequence, the electrical torque may be controlled simply by regulating the active current I_{sq}.

$$T_e = \frac{P}{2}[\Psi_{PM} i_{sq} - (L_d - L_q) i_{sd} i_{sq}] \tag{6}$$

$$T_e = \frac{P}{2}[\Psi_{PM} i_{sq}] \tag{7}$$

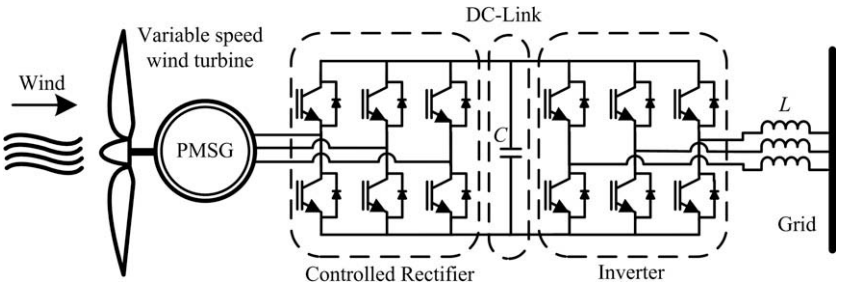

Fig. 1. General scheme of the wind energy conversion system.

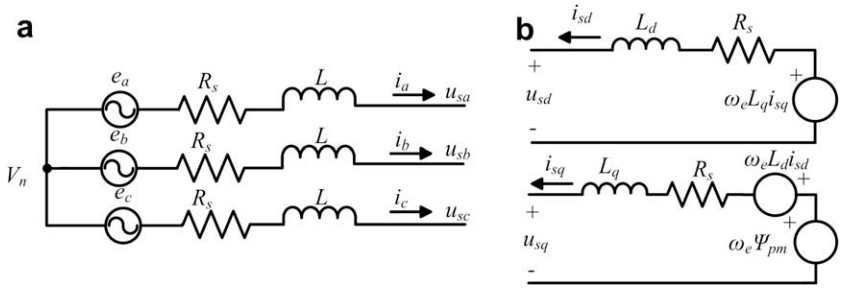

Fig. 2. Equivalent circuits of a PMSG: (a) in a stationary three-phase reference frame and (b) in a synchronous reference frame.

2.2. Wind turbine model

The power generated by the turbine follows Eq. (8), where ρ is the density of the air, r is the wind turbine ratio, V_w is the wind speed, and $C_p(\lambda)$ is the power coefficient, which depends on the tip-speed-ratio parameter, λ. $C_p(\lambda)$ strongly depends on the wind turbine aerodynamics [17] and it has been modeled following Eqs. (9) and (10), respectively, where ω is the turbine rotational speed expressed in *rad/s*. It is worth pointing out that *a, b, c, d, e* and *f* parameters are constant if a fixed pitch angle is considered.

$$P_r = \frac{1}{2}\rho\pi r^2 c_p(\lambda) V_w^3 \tag{8}$$

$$C_p(\lambda) = a + b\lambda + c\lambda^2 + d\lambda^3 + e\lambda^4 + f\lambda^5 \tag{9}$$

$$\lambda = \frac{r\omega}{V_w} \tag{10}$$

From Eq. (8), it may be obtained the expression of the turbine torque, T_r, following Eq. (11).

$$T_r = \frac{1}{2}\rho\pi r^3 c_q(\lambda) V_w^2 \tag{11}$$

where $C_q(\lambda)$ is the torque coefficient, which follows Eq. (12).

$$C_q(\lambda) = \frac{c_p(\lambda)}{\lambda} \tag{12}$$

Fig. 3 shows the aspect of both $C_p(\lambda)$ and $C_q(\lambda)$ characteristics as a function of the tip-speed ratio. Note that both power and torque coefficients are non-dimensional terms.

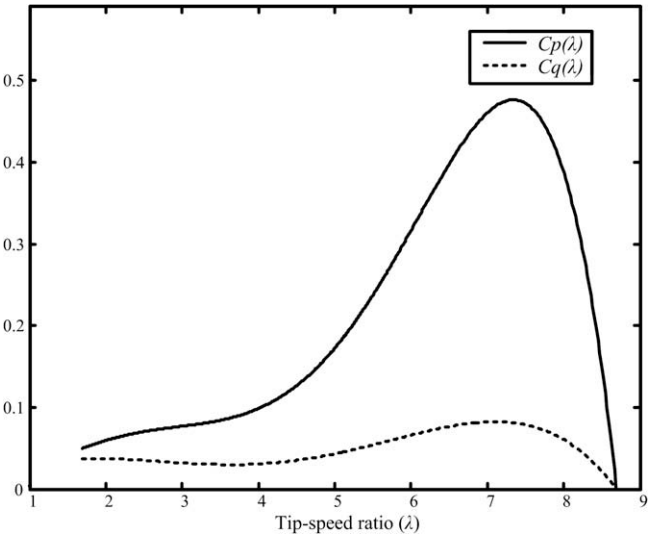

Fig. 3. Power and torque coefficients vs. tip-speed ratio characteristics.

The whole mechanical system is composed by both the wind turbine and the PMSG, with a global dynamic response that follows Eq. (13). J is the turbine and rotor system inertia in kg m/s^2, B_r is the friction coefficient that will be insignificant for the later analysis, T_r is the wind turbine torque, and T_e is the PMSG electromagnetic torque. By considering small-signal variations around an operation point and neglecting the friction term, it results Eq. (14), where s is the variable of the Laplace transform. It is worth pointing out that, in the control of motor drives based on permanent magnet synchronous machines, T_r is normally considered as a disturbance input of the system. However, in the case of WECS, the mechanical torque strongly depends on the PMSG speed, as Eqs. (10)–(12) express. Therefore, the mechanical torque should not be considered as an external disturbance.

Note that in this section each of the variables, say x, is composed by the sum of its DC value at the operation point, X, plus its dynamic small-signal value, $\tilde{x}(s)$, following the expression: $x = X + \tilde{x}(s)$.

A linear expression of T_r can be derived by means of a first order Taylor series, as Eq. (15) expresses. Note that $\widetilde{T}_r$ has a term associated to the wind speed and another one that depends on the generator speed. The wind speed is the true disturbance input of the system, while an intrinsic feedback path will result from the first term of Eq. (16). Starting from Eqs. (9)–(11), the expression of $\widetilde{T}_r$ may be calculated, following Eq. (16). Besides, from Eq. (7) it can be obtained the expression of the electromagnetic torque in the small-signal sense, following Eq. (17).

The electric power that it is processed by the rectifier follows Eq. (18), in which the generator losses have been taken into account. By linearizing Eq. (18) around an operation point, it results Eq. (19).

$$J\frac{d\omega}{dt} = T_r - T_e - B_r\omega \tag{13}$$

$$\tilde{\omega} = \frac{1}{Js}(\widetilde{T}_r - \widetilde{T}_e) \tag{14}$$

$$\widetilde{T}_r = \left.\frac{\partial[T_r(\omega, v_w)]}{\partial\omega}\right|_{\substack{\omega = W \\ v_w = V_w}} \cdot \tilde{\omega} + \left.\frac{\partial[T_r(\omega, v_w)]}{\partial v_w}\right|_{\substack{\omega = W \\ v_w = V_w}} \cdot \tilde{v}_w \tag{15}$$

$$\widetilde{T}_r|_{\tilde{v}_w=0} = \frac{1}{2}\rho\pi r^3 V_w^2\left(-\frac{aV_w}{rW^2} + \frac{cr}{V_w} + \frac{2dr^2W}{V_w^2} + \frac{3er^3W^2}{V_w^3} + \frac{4fr^4W^3}{V_w^4}\right)\cdot\tilde{\omega} \tag{16}$$

$$\widetilde{T}_e = \left.\frac{\partial[T_e(i_{sq})]}{\partial i_{sq}}\right|_{i_{sq}=I_{sq}} \cdot \tilde{i}_{sq} = \frac{P}{2}\Psi_{PM}\tilde{i}_{sq} \tag{17}$$

$$P_{out} = \frac{P}{2}\Psi_{PM} i_{sq}\omega - R_s i_{sq}^2 \tag{18}$$

$$\widetilde{P}_{out}(s) = \frac{P}{2}\Psi_{PM} I_{sq}\tilde{\omega}(s) + \left(\frac{P}{2}\Psi_{PM}W - 2R_s I_{sq}\right)\tilde{i}_{sq} \tag{19}$$

3. Description of the proposed control scheme for WECS

Fig. 4 shows the proposed control scheme for a WECS driven by a back to back converter. The grid side inverter regulates the voltage at the dc-link and injects into the grid the energy that it is extracted from the wind turbine by the rectifier. The analysis of the grid side inverter is out of the scope of this paper, but a detailed description may be found in [14]. Regarding the rectifier, two internal control loops regulate independently the PMSG active and reactive currents, i_{sq} and i_{sd}, respectively, to simultaneously impose $I_{sd} = 0$ and regulate the generator torque. The reference for the active current loop, i.e., for the desired torque, is the output of the cascade connected speed controller. Therefore, the torque response strongly depends on the size of the speed changes. Finally, the reference for the speed control loop depends on the operation mode of the wind turbine. In the MPPT region, the speed reference is calculated by the P&O algorithms to extract as much power as possible from the wind. In CPR, a power loop maintains the generator power to its nominal value, ignoring the MPPT algorithm.

Starting from Eqs. (14)–(19), a block diagram of the whole rectifier control scheme may be obtained, as Fig. 5 shows. As the inner current loops are much faster than both the speed and the power loops, they will be considered as ideal for the analysis that follows, i.e., $\tilde{i}_{sq} \approx \tilde{i}_{qref}$ in Fig. 5. The design of T_{iq} is out of the scope of this paper, but details about this issue may be found in [14].

3.1. Design of the speed control loop

The transfer function from the active current reference to the generator speed may be obtained from Fig. 5, as Eq. (20) expresses. Note that a right half plane pole may appear in this transfer function for certain values of $\lambda = r\omega/V_w$, so that a careful design of the speed controller is mandatory to avoid the system to become unstable. If $\tilde{T}_r$ were considered just as a disturbance input, the transfer function from $\tilde{i}_{sq}$ to $\tilde{\omega}$ would be simplified following Eq. (21). Fig. 6 shows the Bode diagrams of the speed loop gain, $T_\omega = PI_\omega \tilde{\omega}(s)/I_{sq}(s)$, by considering both the accurate and the simplified transfer function from $\tilde{i}_{sq}$ to $\tilde{\omega}$. In the case of the accurate model, several values of λ have been considered. The proportional and integral terms for the chosen PI speed controller, PI_ω, are $k_p = -1$ and $k_i = -25$, respectively. The values of the parameters of the WECS under study are shown in Appendix A.

$$\left.\frac{\tilde{\omega}(s)}{\tilde{i}_{sq}(s)}\right|_{\tilde{v}_w=0} \approx \left.\frac{\tilde{\omega}(s)}{\tilde{i}_{qref}(s)}\right|_{\tilde{v}_w=0} = \frac{-\frac{P}{2J}\Psi_{PM}}{s - \frac{1}{2J}\rho\pi r^3 V_w^2\left(-\frac{aV_w}{rW^2} + \frac{cr}{V_w} + \frac{2dr^2W}{V_w^2} + \frac{3er^2W^2}{V_w^3} + \frac{4fr^4W^3}{V_w^4}\right)} \tag{20}$$

$$\left.\frac{\tilde{\omega}(s)}{\tilde{i}_{sq}(s)}\right|_{\tilde{v}_w=0,\tilde{T}_r=0} = \frac{-\frac{P}{2J}\Psi_{PM}}{s} \tag{21}$$

Note from Fig. 6 the sensitivity of the speed control loop to variations of λ, it is observed that the stability of the speed control system could be compromised if an excessively low crossover frequency is chosen. Moreover, wrong conclusions about the system stability may be extracted if the designer performs the analysis by means of the simplified model. Although both the accurate and the simplified model agree at high frequencies, at medium and low frequencies the actual response of the wind turbine strongly depends on λ, differing from the one predicted by the simplified model. It seems that this problem may be solved by choosing a high enough crossover frequency for the speed loop. However, the generator speed will respond quickly to changes in the reference for high values of the T_ω crossover frequency. Therefore, if an excessively high crossover frequency is chosen, the resulting 'aggressiveness' of the speed loop produces an abrupt torque response that could damage the mechanical transmission of the system. As a conclusion, the choice of the speed loop crossover frequency results from a compromise between the explained issues.

The dynamic response of the rotational speed to changes in the reference can be obtained by calculating the expression of the speed closed control loop as expressed by Eq. (22). Note that the wind speed is considered as a disturbance of the system.

$$\left.\frac{\tilde{\omega}(s)}{\tilde{\omega}_{ref}(s)}\right|_{\tilde{v}_w=0} = \frac{-\frac{P}{2J}\Psi_{PM}\left(s + \frac{k_i}{k_p}\right)}{\frac{s^2}{k_p} - \frac{s}{2J}\left[P\cdot\Psi_{PM} + \frac{\rho\pi r^3 V_w^2}{k_p}\left(-\frac{aV_w}{rW^2} + \frac{cr}{V_w} + \frac{2dr^2W}{V_w^2} + \frac{3er^3W^2}{V_w^3} + \frac{4fr^4W^3}{V_w^4}\right)\right] - \frac{Pk_i}{2Jk_p}\Psi_{PM}} \tag{22}$$

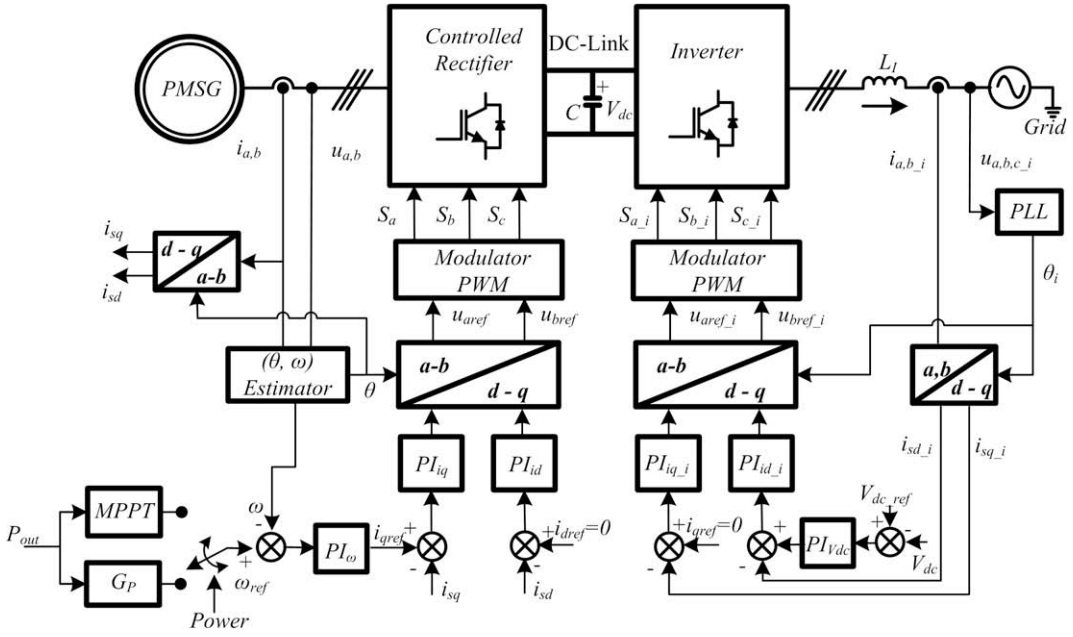

Fig. 4. Scheme of the WECS control stage.

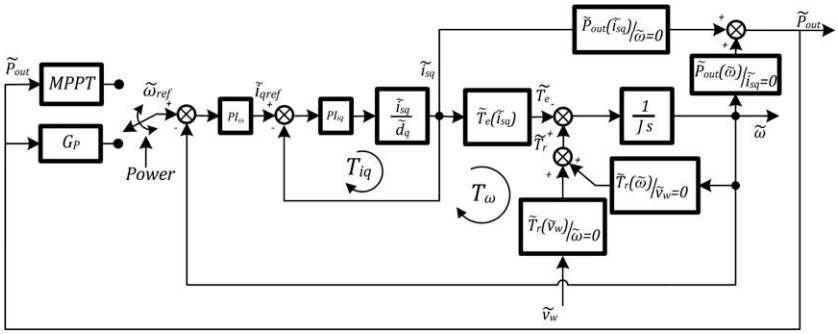

Fig. 5. Block diagram of the whole rectifier control scheme.

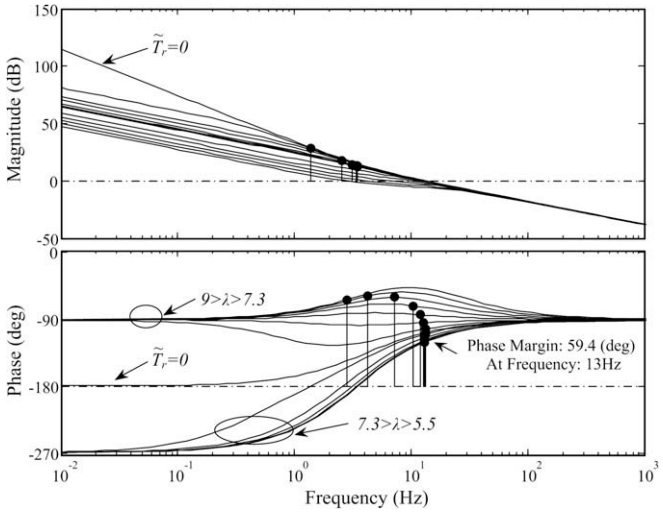

Fig. 6. Bode plots of the speed control loop gain, T_ω.

To close the speed control loop, the rotational speed of the generator must be measured or estimated by means of some kind of sensorless technique. Several estimation methods have been proposed in the past [18]. In this work, a simplified Kalman observer (SKO) [19], has been chosen to estimate the rotational speed starting from the measurement of the generator voltages and currents. The SKO algorithm has a variable reduced state vector and a constant gain matrix. In the particular case of a PMSG, the SKO input variables are the estimation of the electromotive force (EMF) in the stationary $\alpha\beta$ reference frame $e_\alpha(n)$, $e_\beta(n)$ following Eq. (23), where $\theta(n)$, $\omega_e(n)$ are the position and EMF speed, and $\acute{w}(n)$ is an auxiliary variable which represents the estimation error.

$$\left.\begin{aligned}
&\varepsilon(n-1) = e_\alpha(n)\cos(\theta(n-1)) - e_\beta(n)\sin(\theta(n-1))\\
&\theta(n) = [\theta(n-1) + T_s\omega_e(n-1) + k_{e1}\varepsilon(n-1)]\\
&\omega_e(n) = \omega_e(n-1) + \acute{w}(n-1) + k_{e2}\varepsilon(n-1)\\
&\acute{w}(n) = \acute{w}(n-1) + k_{e3}\varepsilon(n-1)
\end{aligned}\right\} \quad (23)$$

The filter gains k_{e1}, k_{e2} and k_{e3} are calculated by using the extended Kalman filter recursive algorithm. In this application, the value of the filter gains has been calculated by means of the *dqlr* MATLAB® function [20], resulting $k_{e1} = 0.0038$, $k_{e2} = 0.7357$ and $k_{e3} = 0.0007$.

3.2. Analysis of the power loop

The transfer function from the speed to the generated power, following Eq. (24), may be obtained from Eqs. (19) and (20). The expression of τ_z in Eq. (24) is detailed in Eq. (25). Note that this transfer function has a Right Half Plan Zero for certain values of τ_z, so that a non minimum phase response is expected. By multiplying Eqs. (22) and (24), the expression of the reference speed to power has been calculated, as expressed by Eq. (26).

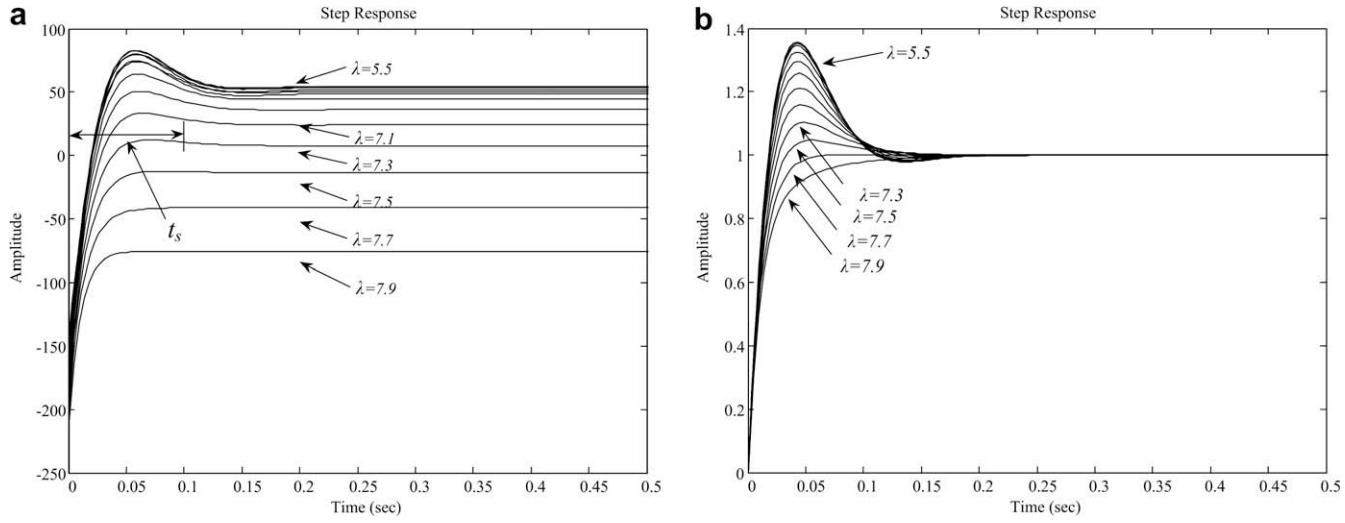

Fig. 7. Response to steps in the reference speed, (a) $\tilde{P}_{out}(s)/\tilde{\omega}_{ref}(s)$ and (b) $\tilde{\omega}(s)/\tilde{\omega}_{ref}(s)$.

$$\left.\frac{\widetilde{P}_{out}(s)}{\tilde{\omega}(s)}\right|_{\tilde{v}_w=0} = -\frac{\left(\frac{P}{2}\Psi_{PM}W - 2R_sI_{sq}\right)}{\frac{P}{2J}\Psi_{PM}}\cdot\left[s - \left(\frac{\frac{I_{sq}}{J}\left(\frac{P}{2}\Psi_{PM}\right)^2}{\frac{P}{2}\Psi_{PM}W - 2R_sI_{sq}} + \tau_z\right)\right] \quad (24)$$

$$\tau_z = \frac{1}{2J}\rho\pi r^3 V_w^2\left(-\frac{aV_w}{rW^2} + \frac{cr}{V_w} + \frac{2dr^2W}{V_w^2} + \frac{3er^3W^2}{V_w^3} + \frac{4fr^4W^3}{V_w^4}\right) \quad (25)$$

$$\left.\frac{\widetilde{P}_{out}(s)}{\tilde{\omega}_{ref}(s)}\right|_{\tilde{v}_w=0} = -\frac{\left(\frac{P}{2}\Psi_{PM}W - 2R_sI_{sq}\right)}{\frac{P}{2J}\Psi_{PM}}\cdot\left[s - \left(\frac{\frac{I_{sq}}{J}\left(\frac{P}{2}\Psi_{PM}\right)^2}{\frac{P}{2}\Psi_{PM}W - 2R_sI_{sq}} + \tau_z\right)\right] \cdot\left(\frac{-\frac{P}{2J}\Psi_{PM}\left(s + \frac{k_i}{k_p}\right)}{\frac{s^2}{k_p} - \frac{Pk_i}{2Jk_p}\Psi_{PM} - s\left[\frac{P}{2J}\Psi_{PM} + \frac{\tau_z}{k_p}\right]}\right) \quad (26)$$

Fig. 7 shows the response of both the power Fig. 7a and the speed Fig. 7b to a step in the speed reference. As it has been previously pointed out, for certain values of λ the power response to changes in the speed reference is the typical one of a non minimum phase system. It is mandatory to take this fact into account when designing the MPPT algorithm, because a wrong sign of the power increments may be measured if an excessively short iteration time is used, so that the algorithm would work improperly. The stabilization time t_s can be easily measured from those plots. This time would be a good choice for the iteration time of the MPPT algorithms. Finally, it may be noted that the stabilization time strongly depends on the response of the speed control loop, as it can be concluded by comparing Fig. 7a and b.

4. Proposed MPPT algorithm

The P&O algorithm is an iterative method which operates in a wide range of wind speeds. It works continuously perturbing the system by increasing and decreasing the speed reference of the speed loop and evaluating the sign of the achieved power response. If a positive power increment is measured, the algorithm maintains the sign of the reference speed steps. Otherwise, the sign of the steps is changed. Several studies carried out on WECS applications show that the P&O algorithm presents disadvantages in systems with high inertia [21]. Concretely, the torque oscillations produced by the continuously changing operation point could damage the mechanical system, especially if its resonance frequency is excited. The proposed solution achieves soft response of the generator torque, so that the risk of damage is dramatically reduced.

Fig. 8 shows the operation sequence of both the conventional [4] and the proposed P&O algorithms. The proposed method is derived from the conventional one by substituting the steps on the speed reference by a ramp signal. The slope of the ramp signal is determined by two factors: the size of the step that would be used in the conventional algorithm, and the stabilization time of the power response to changes in the reference speed.

5. Simulation results

To evaluate the performance of the proposed technique, it has been applied to a WECS with the parameters shown by Appendix A. A simulation study has been carried out by means of PSIM© software [22], which allows programming the whole control algorithms in C code by using an embedded script block. To

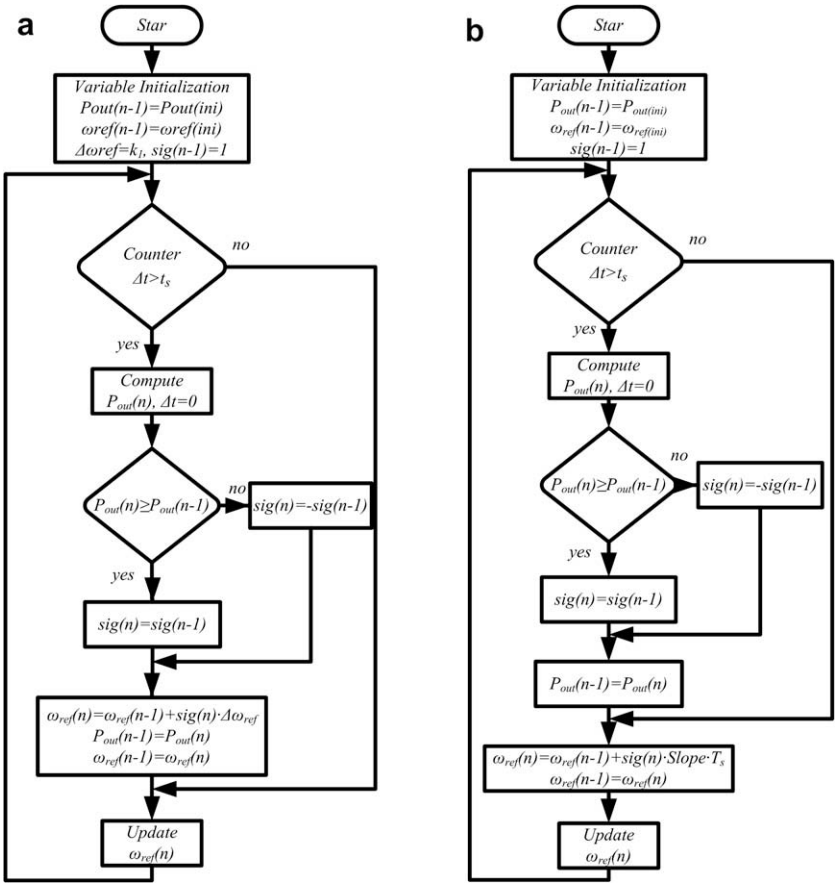

Fig. 8. Flowchart of P&O algorithms, (a) conventional algorithm and (b) proposed algorithm.

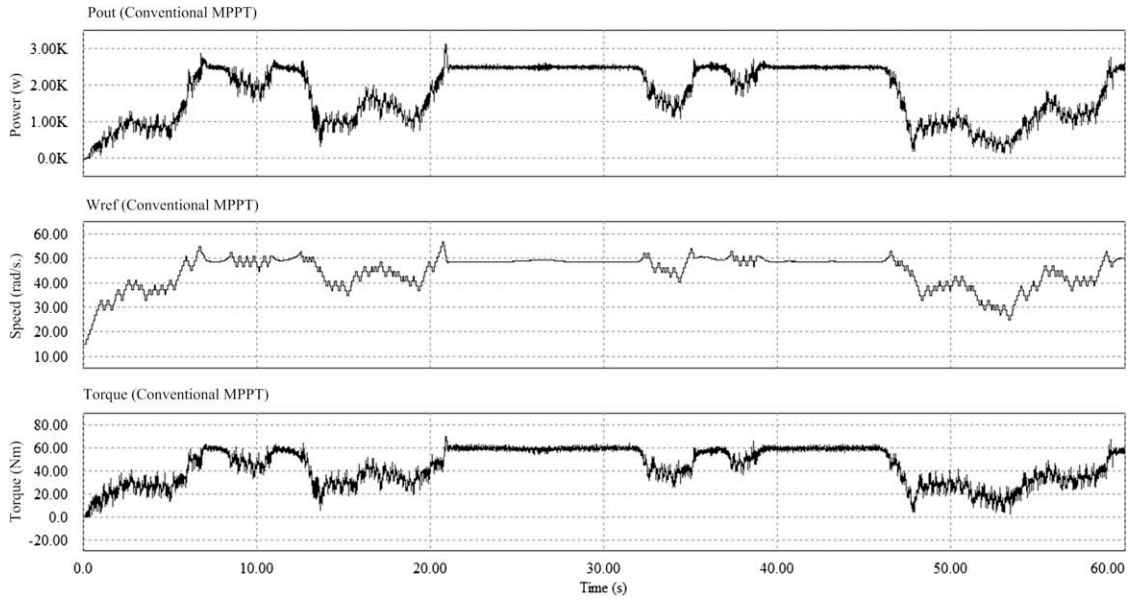

Fig. 9. Evolution of the generated power (up), of the reference speed (middle) and of the turbine torque (down) with conventional P&O.

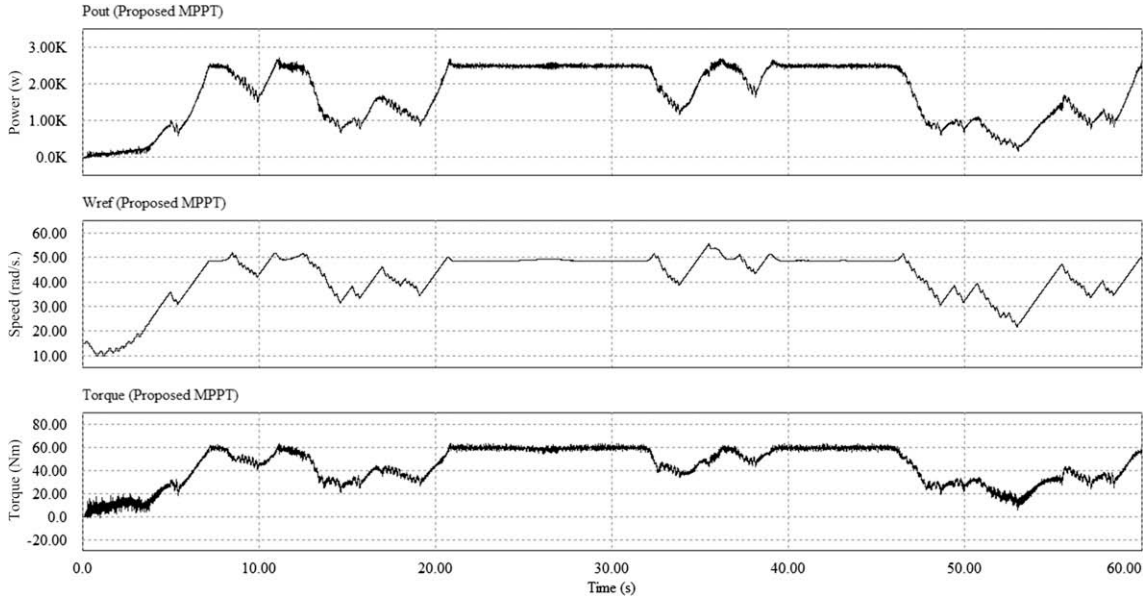

Fig. 10. Evolution of the generated power (up), of the reference speed (middle) and of the turbine torque (down) with proposed P&O.

emulate the wind fluctuations and compare the performance of both the conventional and the proposed P&O algorithms, a wind profile without turbulences and without taking into account the tower shadow effect has been defined, as Eq. (27) expresses. The frequency ω_r depends on the desired test time, following Eq. (28). In this case, a test time $t_{test} = 60$ s has been chosen.

Fig. 9 shows the evolution of the generated power, of the reference speed and of the mechanical torque by using the conventional P&O algorithm to achieve MPPT. Fig. 10 shows the evolution of the same variables, measured in the same conditions, by using the proposed P&O technique. Note that both the speed and the torque ripples are significantly decreased by applying the proposed algorithm. From another point of view, the average value of the generated power has been calculated by using both algorithms, following Eqs. (29) and (30). Note that no significant differences have been measured.

$$v_w(t) = 10 + 2 \cdot \sin(\omega_r t) + 2 \cdot \sin(3.5 \cdot \omega_r t) + \sin(12.5 \cdot \omega_r t) + 0.2 \cdot \sin(35 \cdot \omega_r t) \quad (27)$$

$$\omega_r = \frac{2\pi}{t_{test}} rad/s \quad (28)$$

$$P_{out(\text{average})} = \frac{1}{t_{test}} \int_0^{t_{test}} (P_{out}) dt \quad (29)$$

$$\frac{P_{out(\text{average})}|_{\text{MPPT proposed}}}{P_{out(\text{average})}|_{\text{MPPT classical}}} \cdot 100\% = 98.25 \quad (30)$$

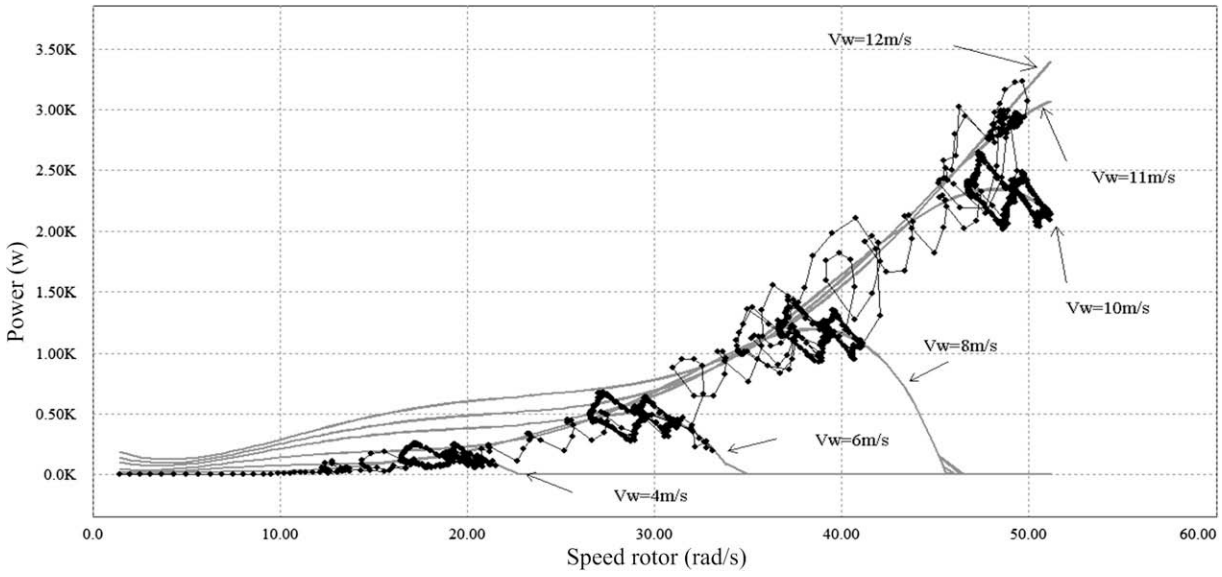

Fig. 11. Response of the conventional P&O algorithm to step changes in the wind speed from 4 m/s to 12 m/s.

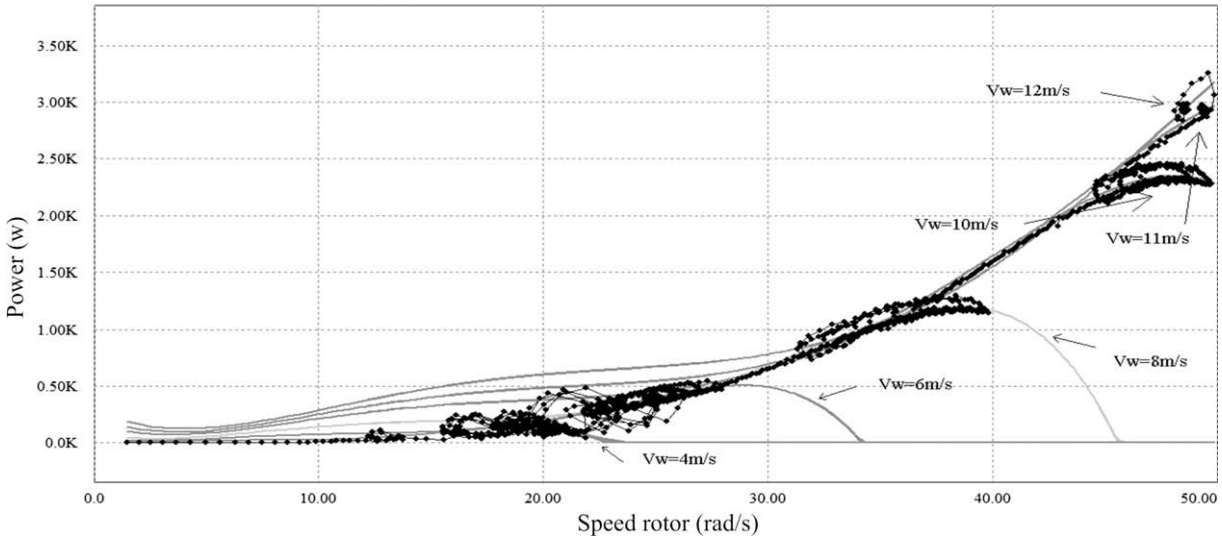

Fig. 12. Response of the proposed P&O algorithm to step changes in the wind speed from 4 m/s to 12 m/s.

Figs. 11 and 12 show the response of both the conventional and the proposed P&O algorithms, respectively, to a succession of sudden wind steps from 4 m/s to 12 m/s. The proposed technique presents a softer response than the conventional one for all cases, with lower oscillations around each operation point.

6. Conclusions

A new MPPT technique for WECS has been proposed and evaluated in this paper. The proposed approach is similar to the well-known P&O algorithm, but a ramp signal instead of a stepped signal is used to modify the reference speed of the generator, obtaining a softer response of the mechanical variables than the typical one of conventional P&O methods. As a result, the mechanical stress that is applied to the power train dramatically decreases, so that both the maintenance needs and MTBF of the WECS are expected to be improved without significantly reducing the system performance.

Appendix A

A.1. Systems parameters

Number of poles (P)	12	Switching frequency	5 kHz
Armature resistance (R_s)	5 Ω	Sampling time (T_s)	10 μs
Armature inductances ($L_d = L_q = L$)	25 mH	Inertia coefficient systems (J)	0.0833 kg m/s^2
Flux linkages coefficient (Ψ_{PM})	0.9022 volt/r/s	Blade radius turbine (r)	1.525 m
DC link voltage	800 V	Density of wind (ρ)	1.08 kg/m^3
Coefficient wind turbine $a = 0.043$, $b = -0.108$, $c = 0.146$, $d = -0.0605$, e = 0.0104, $f = -0.0006$			

References

[1] Yang H, Wei Z, Chengzhi L. Optimal design and techno-economic analysis of a hybrid solar–wind power generation system. Appl Energy 2009;86(2):163–9.

[2] Camblong H, Martinez de Alegria I, Rodriguez M, Abad G. Experimental evaluation of wind turbines maximum power point tracking controllers. Energy Convers Manage 2006;47(18):2846–58.

[3] Hong YY, Lu SD, Chiou CS. MPPT for PM wind generator using gradient approximation. Energy Convers Manage 2009;50(1):82–9.

[4] Koutroulis E, Kalaitzakis K. Design of a maximum power tracking system for wind-energy-conversion applications. IEEE Trans Ind Electron 2006;53(2):486–94.

[5] Nagai BM, Ameku K, Roy JN. Performance of a 3 kW wind turbine generator with variable pitch control system. Appl Energy 2009;86(9):1774–82.

[6] Salas V, Olías E, Barrado A, Lázaro A. Review of the maximum power point tracking algorithms for stand-alone photovoltaic systems. Sol Energy Mater Sol Cells 2006;90(11):1555–78.

[7] Eakburanawat J, Boonyaroonate I. Development of a thermoelectric battery-charger with microcontroller-based maximum power point tracking technique. Appl Energy 2006;83(7):687–704.

[8] Arifujjaman Md, Tariq Iqbal M, Quaicoe JE. Energy capture by a small wind-energy conversion system. Appl Energy 2008;85(1):41–51.

[9] Neammanee B, Krajangpan K, Sirisumrannukul S, Chatratana S. Maximum peak power tracking-based control algorithms with stall regulation for optimal wind energy capture. IEEJ Trans Ind Appl 2008;128(4):411–7.

[10] Molina MG, Mercado PE. A new control strategy of variable speed wind turbine generator for three-phase grid-connected applications. In: Transmission and distribution conference and exposition, IEEE/PES, Bogota, Colombia; August 13–15, 2008.

[11] Morren J, Pierik J, de Haana SWH. Inertial response of variable speed wind turbines. Electr Power Syst Res 2006;76(11):980–7.

[12] Harnefors L. Speed estimation from noisy resolver signal. In: 6th international conference on power electronics and variable speed drives, PEVD'96, Nottingham, England; September 23–25, 1996.

[13] Gonzalez LG, Figueres E, Garcera G, Carranza O, Gonzalez-Espin F. Modelling and control in wind energy conversion systems (WECS). In: 13th international European conference on power electronics and applications, EPE2009, Barcelona, Spain; September 8–10, 2009.

[14] Figueres E, Garcerá G, Sandia J, González-Espín F, Rubio JC. Sensitivity study of the dynamics of three-phase photovoltaic inverters with an LCL grid filter. IEEE Trans Ind Electron 2009;56(3):706–17.

[15] Yin M, Li G, Zhou M, Zhao C. Modeling of the wind turbine with a permanent magnet synchronous generator for integration. In: IEEE power engineering society general meeting, Tampa, Florida; June 24–28, 2007.

[16] Michalke G, Hansen AD, Hartkopf T. Control strategy of a variable speed wind turbine with multipole permanent magnet synchronous generator. In: European wind energy conference, EWEC2007, Milan, Italy; May 1–7, 2007.

[17] Bhowmik S, Spée R, Enslin JHR. Performance optimization for doubly fed wind power generation systems. IEEE Trans Ind Appl 1990;35:949–58.

[18] Brahmi J, Krichen L, Ouali A. A comparative study between three sensorless control strategies for PMSG in wind energy conversion system. Appl Energy 2009;86(9):1565–73.

[19] Gonzalez LG, Figueres E, Garcera G, Carranza O, Gonzalez-Espin F. Synchronization techniques comparison for sensorless control applied to wind energy conversion systems (WECS). In: 13th international European conference on power electronics and applications, EPE2009, Barcelona, Spain; September 8–10, 2009.

[20] Liu Y, Qiang Zhu Z, Howe D. Instantaneous torque estimation in sensorless direct-torque-controlled brushless DC motors. IEEE Trans Power Electron Appl 2006;42(5):1275–83.

[21] Yaoqin J, Zhongqing Y, Binggang C. A new maximum power point tracking control scheme for wind generation. In: International conference on power system technology, PowerCon 2002 IEEE-PES/CSEE, Kunming, China; October 13–17 2002.

[22] PSIM 7.0 user's guide (2006), Powersim Inc.; March 2006.